

# Exploring Time-Resolved Multiphysics of Active Plasmonic Systems with Experiment-Based Gain Models

Shaimaa I. Azzam, Jieran Fang, Jingjing Liu, Zhuoxian Wang, Nikita Arnold, Thomas A. Klar, Ludmila J. Prokopeva, Xiangeng Meng, Vladimir M. Shalaev, and Alexander V. Kildishev\*

**A systematic approach to investigate lasing and net amplification in plasmonic structures with a finite-difference time-domain method coupled to the rate equations of four-level and six-level atomic systems is developed. The experiment-fitted kinetic parameters are fed into the model to study the mechanism of the coupling of metamaterials and metasurfaces with the gain medium. With the help of such an accurate model, net amplification can be distinguished from time-resolved lasing dynamics for the plasmonic systems coupled with gain.**

## 1. Introduction

The emerging field of plasmonics has stimulated the development of composite optical materials and transformative nanophotonic devices with potential for significant societal and technological impact.<sup>[1]</sup> The fundamental requirement in all these applications is to route and manipulate photons actively at the nanoscale.<sup>[2]</sup> Therefore, there is a high demand for coherent nanoscale optical sources in high-speed and deeply integrated photonic circuits.<sup>[3,4]</sup> While all-dielectric optical sources are restricted by the diffraction limit, surface plasmons (SPs), the oscillations of free electrons in plasmonic materials (e.g., the noble metals), allow us to overcome the diffraction limit with the subwavelength confinement of light. On the other hand, losses

introduced by electron scattering in metals can greatly degrade the performance of a plasmonic system. As a result, active plasmonic devices can be designed by combining a plasmonic material (i.e., metal) and a gain medium (i.e., organic dyes, quantum wells, quantum dots, etc.) to either just compensate for metal losses,<sup>[5,6]</sup> or to create nanoscale coherent light generation with SP amplification by stimulated emission of radiation (spaser).<sup>[7–9]</sup> Overcoming the diffraction

limit with plasmonic nanostructures in spasers is used in several ways. First, replacing a reflective resonator built on a photonic mode (of the wavelength scale) inside a dielectric cavity by a resonator based on a plasmonic mode (of the subwavelength scale) confined at the surface of the metal nanoparticle, substantially reduces the spaser dimensions. Also, the feedback loop in the spaser provided by the near-field interaction between the metal and gain parts of the structure along with the high scattering cross section offered by the plasmonic structures is utilized to form plasmonic random lasers, or random spasers.<sup>[10]</sup> So far, numerous active studies of the spaser have been reported. The first nanoscale coherent generation of SPs was reported in ensemble measurements for Au nanospheres with dielectric gain shells randomly suspended in water.<sup>[9]</sup> In addition, a great number of diverse spaser configurations has been explored, such as nano-wires,<sup>[11,12]</sup> coaxial pillars,<sup>[13]</sup> nano-cavity arrays,<sup>[14–16]</sup> as well as novel lasing mechanisms and feedback such as lasing using stopped-light,<sup>[17]</sup> lasing via plasmonic leaky modes,<sup>[18]</sup> etc. All of them have revealed line-width narrowing and nonlinear output behavior under optical pumping. Perhaps, the very initial use of periodic nano-cavity arrays dates back to 2000 when Vučković et al.<sup>[19,20]</sup> used a silver nanohole array to enhance LED efficiency. Just a few years later, Stuart<sup>[21]</sup> got a patent to use a similar structure for lasing. Vučković–Stuart's design was successfully implemented for a lasing device by van Beijnum et al.<sup>[8]</sup> with InGaAs as a gain material, though no gain was used inside the nanoholes due to fabrication constraints. Simultaneously, an organic injection lasing utilizing gold nano-disc arrays was demonstrated in ref. [22].

Along with lasing, gain media are also used to compensate losses in nanoplasmonic devices.<sup>[5,6,23]</sup> If gain is introduced to the system, one can observe amplified SPs coupled with photons. This would allow efficient plasmonic interconnects and low-loss metamaterial structures. The amplification of SPs and full

S. I. Azzam, Dr. J. Fang, Dr. J. Liu, Dr. Z. Wang, Dr. L. J. Prokopeva, Prof. X. Meng, Prof. V. M. Shalaev, Prof. A. V. Kildishev  
School of Electrical and Computer Engineering and Birk  
Nanotechnology Center  
Purdue University  
West Lafayette, IN 47907, USA  
E-mail: kildishev@purdue.edu

Dr. N. Arnold<sup>[†]</sup>, Prof. T. A. Klar  
Institute of Applied Physics  
Johannes Kepler University  
Altenberger Straße 69, 4040 Linz, Austria

Prof. X. Meng  
Department of Materials Science and Engineering  
Qilu University of Technology  
Jinan 250353, China

[†] Present address: Institute of Experimental Physics/Soft Matter Physics, Johannes Kepler University, Altenberger Straße 69, 4040 Linz, Austria

The ORCID identification number(s) for the author(s) of this article can be found under <https://doi.org/10.1002/lpor.201800071>

DOI: 10.1002/lpor.201800071

compensation of optical losses have been proposed in various plasmonic devices such as long-range surface plasmon polariton (SPP) waveguide,<sup>[24]</sup> active split-ring resonators,<sup>[25,26]</sup> and active negative index metamaterials<sup>[6,27]</sup> studied in time and frequency domains.<sup>[28–30]</sup>

In order to unlock the temporal details of the spaser and SP amplifier, numerous theoretical and numerical methods have been proposed.<sup>[31–33]</sup> Among them, due to the accurate treatment of quantum properties of the gain medium, the time-domain multiphysics approach is viewed as the most powerful method, in which a finite-difference, finite-volume, or a finite element time-domain method is coupled to a multi-level system through auxiliary differential equations.<sup>[34]</sup> Using a classical FDTD scheme, this approach has been applied to investigate lasing dynamics,<sup>[35–37]</sup> and interpret lasing experiments.<sup>[14,32]</sup> Recently, the Maxwell-Bloch-Langevin (MBL) approach has been introduced and broadly used by the Hess group<sup>[38–40]</sup> to account for the spatial and temporal fluctuations providing a more accurate means of simulating amplified spontaneous emission. For example, the use of the MBL approach provided insight on the lasing dynamics in an active nanofishnet structure,<sup>[39]</sup> indicating that the bright mode is subject to a nonlinear competition with the dark plasmonic mode, leading to a steady-state emission where bright and dark modes coexist and could be used to control the system. Adding the concept of the stopped-light to plasmonic nanolasing<sup>[17]</sup> and employing the MBL approach allows us to perform a detailed study of the spatio-temporal dynamics of coherent amplification and lasing.<sup>[40]</sup>

Although most of the simulations provide self-consistent results, few works simulate lasing dynamics using kinetic parameters directly retrieved from the analysis of the gain media.<sup>[41]</sup> In addition, all these schemes rely on a four-level atomic system which may not be accurate enough in some more complex gain media that exhibit non-negligible split transitions, for example, organic dyes.<sup>[42]</sup> In this work, we provide a detailed study on lasing and net amplification for plasmonic devices with gain. First, we use a model developed here to investigate and confirm our recent experimental work on lasing from silver nanohole arrays coated with Rhodamine-101 (R101) dye.<sup>[16]</sup> Then, we investigate the compensation of SPP losses in a Kretschmann–Raether configuration with adjacent Firefli\*fluorescent green dye.<sup>[42]</sup> However, the approaches used here can be applied to general cases of modeling active plasmonics with multi-level gain systems.

To address the need for modeling the gain media in time-domain accurately, we study solid films of the organic dyes (R101 and fluorescent green dye) using a pump–probe setup and match the measurements with the numerical models to retrieve the kinetic parameters of the dyes. The pump–probe results indicate the dependence of population inversion and effective gain on the pumping power. The retrieved kinetic parameters are then fed into a full-wave FDTD model to study the dynamic process in the plasmonic and gain medium coupled systems.<sup>[16,23]</sup> For both experiments and numerical models, we observed net amplification and fast gain saturation which is directly linked to the plasmonic field enhancement. For the silver nanohole array, as more gain is introduced to the coupled system, the simulated emission shows a clear lasing threshold behavior matched with the experiment. We observe the clamping of the population inversion and consequently gain depletion which manifests as coherent emis-

sion of SPs. Furthermore, for the Kretschmann–Raether configuration, no lasing can be observed due to the absence of feedback. Therefore, as the gain in the system is increased, clamping of the population inversion and consequent gain depletion occur, but in this case it corresponds to the amplification of the SPPs and hence loss compensation is attained. We believe our time-domain simulations with calibrated kinetic parameters are particularly instrumental for acquiring insight in the time dynamic physics of plasmonic structures/nanostructures with gain. The remainder of this paper is organized as follows: after presenting the kinetic models of four and six-level systems in Section 2, we also provide a brief comparison of their similarities and differences. We then proceed with the review of primary results and their analysis in Section 3 as we apply the proposed model to two different systems where net gain and lasing are studied.

## 2. Theoretical Models

The interaction between the electromagnetic field and the gain medium is modeled using a semi-classical approach in which the atoms/molecules of the gain medium are treated quantum mechanically using a four-level or a six-level quantum system based on the type of the dye (shown in **Figure 1**), and the electromagnetic waves are treated classically with Maxwell's equations.

### 2.1. Four-Level System

Four-level quantum system is shown in **Figure 1a**. Total population density of the non-excited atoms or molecules of the gain medium  $N$  are generally initially hosted in the ground level  $|0\rangle$ . They can then be pumped with the Gaussian pump pulse to the highest level  $|3\rangle$ . A fast non-radiative transition occurs between the highest level  $|3\rangle$  and upper lasing level  $|2\rangle$ . Molecules can be transferred from the upper to the lower lasing levels (from  $|2\rangle$  to  $|1\rangle$ ) via spontaneous and stimulated emissions. A proper coupling between gain medium and substantial local field enhancement might result in population inversion between energy levels  $|2\rangle$  and  $|1\rangle$ , where the stimulated lasing action is intended to take place.

We assume that initially the system is at the ground level  $|0\rangle$ . Population density at a given energy level  $E_i$  varies with time and position  $N_i(\mathbf{r}, t)$ , where  $i \in \{1, 2, 3, 4\}$ . The total population is universally conserved:  $N_0(\mathbf{r}, t) + N_1(\mathbf{r}, t) + N_2(\mathbf{r}, t) + N_3(\mathbf{r}, t) = N$ .

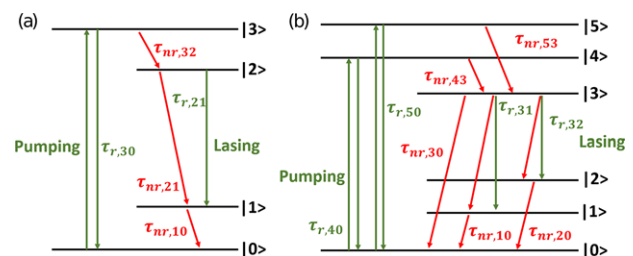


**Figure 1.** Scheme of a population transfer process of the a) four-level and b) six-level systems for an optically excited dye molecule and the governing rate equations.

The system's relaxation from higher to lower levels follows an exponential decay, where upward transitions can be neglected in the visible energy range (due to detailed balance and Boltzmann distribution). Then the dynamics of the population densities at different energy levels shown in Figure 1a satisfies Equation (1) (SI units are used throughout this paper)

$$\begin{cases} \dot{N}_3 = -\tau_{32}^{-1} N_3 + f_{30} \\ \dot{N}_2 = -\tau_{21}^{-1} N_2 + \tau_{32}^{-1} N_3 + f_{21} \\ \dot{N}_1 = -\tau_{10}^{-1} N_1 + \tau_{21}^{-1} N_2 - f_{21} \\ \dot{N}_0 = \tau_{10}^{-1} N_1 - f_{30} \end{cases} \quad (1)$$

Time evolution of the population densities at different levels  $N_i$  is governed by the relaxations (with “-”) from an upper level to a lower level, the inflow rate (with “+”) to a lower level population due to relaxation from an upper level, and the transition rate due to stimulated energy transfer between electromagnetic fields and the gain medium. Only the dominant relaxation channels with a decay time  $\tau_{ij}$  for each  $ij$  level pair are included. They have both radiative and non-radiative contributions defined as  $\tau_{ij}^{-1} = \tau_{r,ij}^{-1} + \tau_{nr,ij}^{-1}$ . In the current model we assume that the relaxation from  $|3\rangle$  to  $|0\rangle$  can be neglected in comparison with the much faster channel  $|3\rangle$  to  $|2\rangle$ .

The driving terms  $f_{ij}$  modeling the stimulated energy transfer are given by Equation (2)<sup>[34]</sup>

$$f_{ij} = \frac{1}{\hbar\omega_{ij}} \mathbf{E} \dot{\mathbf{P}}_{ij}, \quad ij \in \{21, 30\} \quad (2)$$

where  $\omega_{ij}$ ,  $\mathbf{P}_{ij}$  are the Lorentzian frequency and the macroscopic polarization of the transition from  $|i\rangle$  to  $|j\rangle$ , respectively. Each macroscopic polarization  $\mathbf{P}_{ij}(r, t)$  satisfies the Lorentz ordinary differential equation given by Equation (3)

$$\dot{\mathbf{P}}_{ij} + \gamma_{ij} \mathbf{P}_{ij} + \omega_{ij}^2 \mathbf{P}_{ij} = \kappa_{ij} [N_j - N_i] \mathbf{E}, \quad ij \in \{21, 30\} \quad (3)$$

where the excitation term is proportional to the difference in populations  $N_j - N_i$ ,  $\gamma_{ij}$  is the dephasing rate for the polarization  $\mathbf{P}_{ij}$ . Here the coupling coefficients are  $\kappa_{ij} = 6\pi\epsilon_0 c^3 / (\tau_{r,ij} \omega_{ij}^2 \sqrt{\epsilon_h})$ , where  $\tau_{r,ij}$  is the radiative lifetime of the transition  $ij$  in the host material and  $\epsilon_h$  is the permittivity of the host medium. It is worth mentioning that the coupling coefficients  $\kappa_{ij}$  are derived from the the dipole matrix element between levels  $|i\rangle$  and  $|j\rangle$  as  $\kappa_{ij} = 2\omega_{ij} \mu_{ij}^2 / \hbar$ .<sup>[34]</sup> It is also important to note that these values of coupling coefficients assume that all the dipoles of the active medium are fully aligned with the field. A more realistic scenario is that the dipoles are randomly oriented and hence the values of the coupling coefficients are three times smaller.

The macroscopic polarization density  $\mathbf{P}(\mathbf{r}, t)$  is coupled to the Maxwell's equations through  $\mathbf{D}(\mathbf{r}, t) = \epsilon_0 \epsilon_h \mathbf{E}(\mathbf{r}, t) + \mathbf{P}(\mathbf{r}, t)$  where  $\epsilon_0$  is the free-space electric permittivity and  $\epsilon_h$  is the relative permittivity of the host material. The rate equations, the macroscopic polarization driving equation, and the Maxwell's equations are then solved in sync within a joined numerical multiphysics framework on a standard FDTD Yee grid, providing a detailed nonlinear interplay between the population dynamics and local electromagnetic fields.

## 2.2. Six-Level System

Spectra of more complex organic dyes exhibits multiple vibronic peaks, therefore, their emission and/or absorption cannot be modeled with a single Lorentzian as in the four-level system. We propose a more realistic six-level kinetic system that can take into account the effect of the non-negligible split transitions in such dyes. This provides a more physical and accurate description of a given gain medium, resulting in a better fit to the experimental measurements of absorption and emission spectra of a given host-embedded dye, which allows for a more detailed analysis of pump-probe experiment dynamics.

Figure 1b shows the dominant considered transitions for the atoms/molecules modeled by the six-level kinetic system which are governed by the rate equations given in Equation (4). Driving terms  $f_{ij}$  and macroscopic polarizations  $\mathbf{P}_{ij}$  are described by Equation (2) and (3), respectively, with  $ij \in \{31, 32, 40, 50\}$ .

$$\begin{cases} \dot{N}_5 = -(\tau_{53}^{-1} + \tau_{50}^{-1}) N_5 + f_{50} \\ \dot{N}_4 = -(\tau_{43}^{-1} + \tau_{40}^{-1}) N_4 + f_{40} \\ \dot{N}_3 = -(\tau_{30}^{-1} + \tau_{31}^{-1} + \tau_{32}^{-1}) N_3 \\ \quad + \tau_{43}^{-1} N_4 + \tau_{53}^{-1} N_5 + f_{31} + f_{32} \\ \dot{N}_2 = -\tau_{20}^{-1} N_2 + \tau_{32}^{-1} N_3 + f_{32} \\ \dot{N}_1 = -\tau_{10}^{-1} N_1 + \tau_{31}^{-1} N_3 - f_{31} \\ \dot{N}_0 = \tau_{10}^{-1} N_1 + \tau_{20}^{-1} N_2 + \tau_{30}^{-1} N_3 \\ \quad + \tau_{40}^{-1} N_4 + \tau_{50}^{-1} N_5 - f_{40} - f_{50} \end{cases} \quad (4)$$

Differences and similarities with respect to our four-level scheme are worth noting. Both absorption and emission initiate from the ground states of the vibronic structures of their electronic levels, but may end at different vibronic levels (highly overlapping with the vibrational wave-function of the initial state). That is why we split only the final states of the electronic transitions. These states then quickly non-radiatively relax to their corresponding vibrational ground states. In principle, the relaxations from  $|3\rangle$  to  $|2\rangle$  and from  $|3\rangle$  to  $|1\rangle$  may have both radiative and non-radiative components, although by far the fastest non-radiative relaxation of the upper lasing level is from  $|3\rangle$  to  $|0\rangle$ , to the bottom of the ground state of the lower electronic level. Similar to four-level scheme, the non-radiative parts of the transitions from  $|5\rangle$  to  $|0\rangle$  and  $|4\rangle$  to  $|0\rangle$  are neglected in our six-level system computations, but could be easily included. This simplification is of little consequence, as  $|5\rangle$  to  $|3\rangle$  and  $|4\rangle$  to  $|3\rangle$  pathways are typically much faster (and faster than the radiative relaxations to level  $|0\rangle$  as well). Coupling between the induced macroscopic polarizations and the Maxwell equations as well as the numerical implementation of the system is the same as in Section 2.1. Following the details of the numerical models presented in this Section, we will proceed with the results of the time-domain modeling of two different plasmonic systems in Section 3.

## 3. Results and Discussion

### 3.1. Parameter Retrieval Using Film Transmission

The samples are R101 dye embedded in a thin film of polyvinyl alcohol (PVA) on an ITO-coated glass substrate and a fluorescent

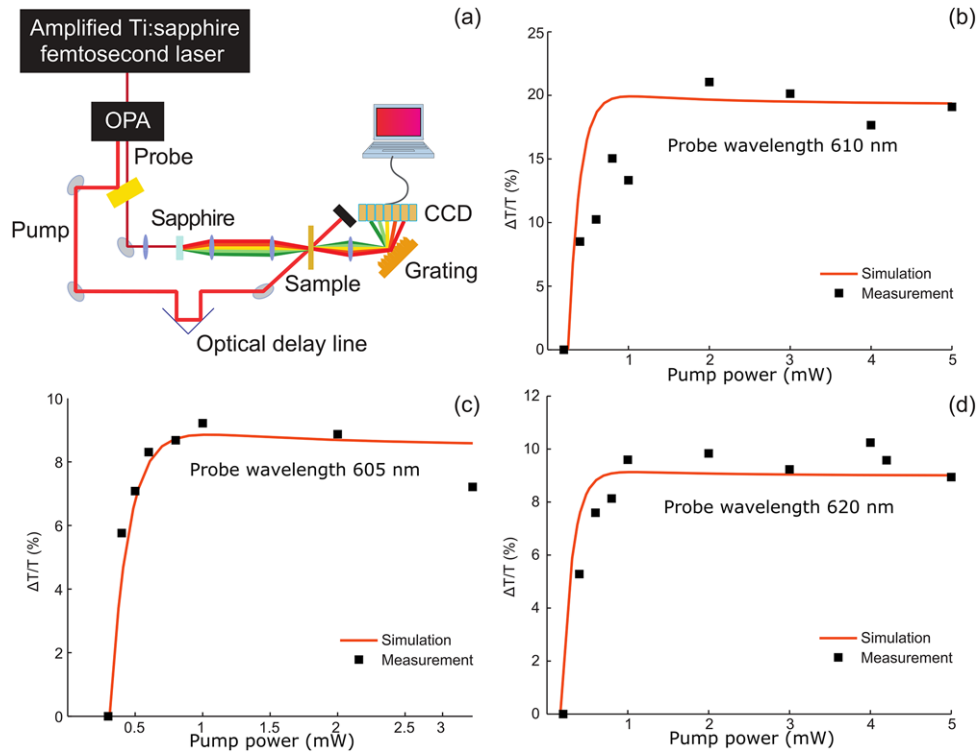


**Figure 2.** a) Pump-probe experimental setup, and saturated transmission results (both measurement and simulation) performed with pump wavelength at 595 nm and probe wavelength at b) 605 nm, c) 610 nm, and d) 620 nm.

green dye in a thin poly(methyl methacrylate) (PMMA) film on a glass substrate. The kinetic parameters of the R101-PVA and the fluorescent green-PMMA film samples are obtained by matching the pump-probe simulations with experiments as they are fitted to four-level and six-level systems, respectively. The scheme for the pump-probe experiment is shown in **Figure 2a** while the detailed setups are explained elsewhere.<sup>[41]</sup> The objective is to feed the retrieved kinetic parameters into a full-wave FDTD model to study the mechanism of the coupling between the plasmonic structures and the gain medium in the net amplification and lasing regimes.

The 2  $\mu\text{m}$ -thick R101-PVA sample is illuminated by two beams, a 595 nm narrow band pump beam and femtosecond

probe beam delayed by 2 ps. Total R101 chromophore density is 10 mM ( $N = 6.0221 \times 10^{24} \text{ m}^{-3}$ ). We calculate the differential transmittance  $\Delta T/T$  by taking the difference of the measured transmittance with and without pumping divided by the transmittance without pumping. This treatment will minimize the influence of the background fluorescence effect which is inevitable in experiments. To improve the fitting fidelity, we run multiple simulations at various pump powers and probe wavelengths. A collection of measurements with corresponding simulations is shown in **Figure 2b-d**. We retrieved the following four-level system parameters: transition wavelengths  $\lambda_{30} = 575 \text{ nm}$  and  $\lambda_{21} = 605 \text{ nm}$ ; dephasing times  $T_{2,30} = 9 \text{ fs}$  and  $T_{2,21} = 25.5 \text{ fs}$ ; decay times  $\tau_{r,30} = 5 \text{ ns}$ ,  $\tau_{nr,32} = 0.3 \text{ ps}$ ,  $\tau_{r,21} = 6 \text{ ns}$ ,  $\tau_{nr,21} = 7.33 \text{ ns}$ ,

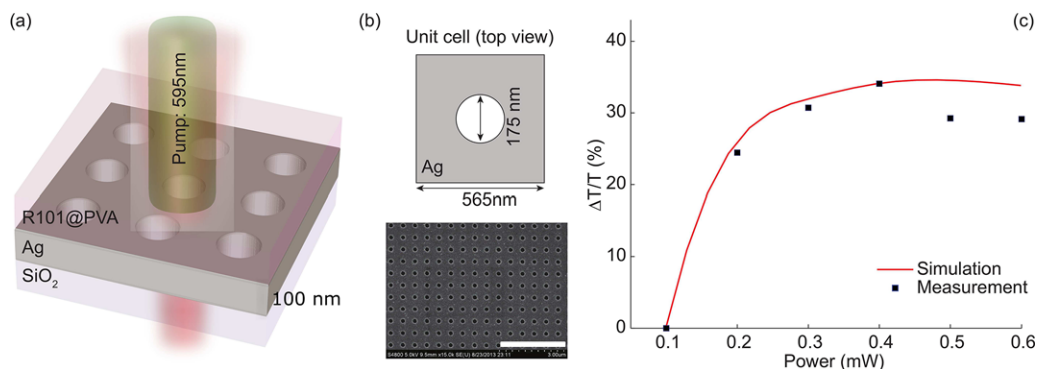


**Figure 3.** a) Schematic view of the silver nanohole array structure covered by R101-PVA film. b) Top view of unit cell and SEM image of the fabricated sample (scale bar: 3  $\mu\text{m}$ ). c) Saturated transmission results of the nanohole array structure (both measurement and simulation) performed with pumping wavelength at 595 nm and probing wavelength 605 nm.

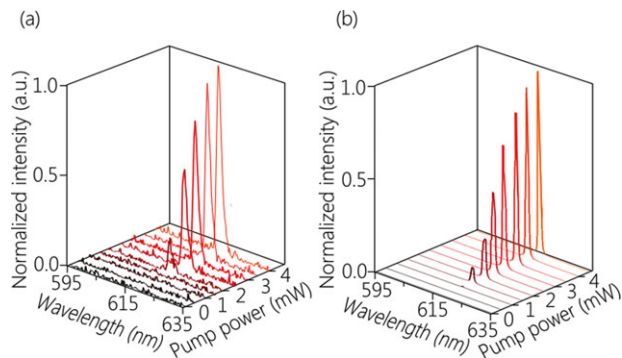


**Figure 4.** Evolution of the emission spectra with increasing pumping power: a) experimental results and b) simulations results.

and,  $\tau_{nr,10} = 0.35$  ps. It is important to note that all simulations have been performed with parameters identical to those obtained from the experiment which are pump and probe pulse durations of 150 fs with a delay between the pump and probe signals of 2 ps and a repetition rate of 1000 Hz. Since there is no resonant feedback involved, we observe a saturation in transmission value with increasing pumping levels that is due to the saturation of pumping transition, which limits the inversion available to the lasing.

### 3.2. Dynamic Processes in the Metal Nanohole Array With Gain

Since dye emission characteristics can depend on the local environment, we re-evaluate the retrieved kinetic parameters for the gain medium incorporated in the nanohole array. The updated kinetic parameters are crucial to the assessment of the dynamic process of net amplification and lasing in the coupled system. The structure considered is an array of metal nanoholes with a periodicity of 565 nm, 175 nm diameter, and 100 nm thickness, which exhibits a resonance around 617 nm,<sup>[16]</sup> close to the emission line (605 nm) of R101. A schematic of the structure and SEM image of the fabricated nanohole array are shown in **Figure 3a,b**. The nanohole array is made of silver with its permittivity modeled by a Drude–Lorentz response which is implemented in the time-domain through a generalized dispersion material (GDM) model.<sup>[43]</sup> The parameters of the Drude–Lorentz model for silver are adapted from an online database.<sup>[44]</sup>

Due to the strong coupling between the pump pulse and gain medium, the plasmonic field enhancement affects the time dependence of the population inversion and subsequently increases the effective gain, leading to a dramatic increase in transmission. This results in rather fast gain saturation, on the order of 0.3 mW, as compared to 1 mW for the bare dye film (see **Figures 3c and 2b**). The probe pulse forms SPP-Bloch waves at the interface between gain medium and silver nanohole array, that is,

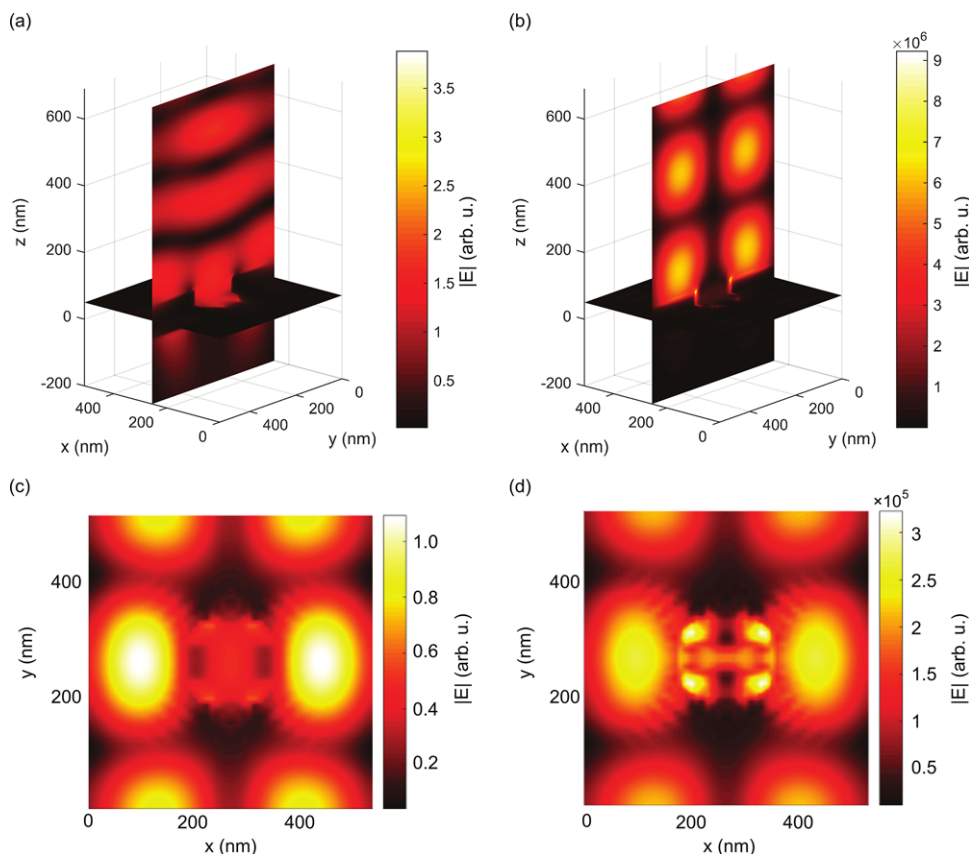


**Figure 5.** The simulated electric field distribution at different pumping powers at the lasing wavelength (617 nm). Cross section view of the time-averaged field distribution for pumping power of a) 0.5 mW and b) 3.5 mW. In-plane view of nanohole array at  $z = 0$  nm for time-averaged field distribution at pumping power of c) 0.5 mW and d) 3.5 mW.

coherent constructive interference of SPP waves scattered at individual nanoholes.<sup>[16]</sup> This strong optical feedback introduces another plasmonic decay channel for the molecules in the excited state and hence depletes these states quickly. Therefore, the retrieval shows a more rapid non-radiative decay rate for the SP-gain coupled system, with the non-radiative lifetime of lasing transition  $\tau_{nr,21}$  reduced from  $\approx 7$  ns to  $\approx 4$  ns, proving the existence of an additional decay channel due to the plasmonic coupling.

To study the dynamic processes in the metal nanohole array with gain, we combine the systematic theoretical model described before with the experiments performed using the same configuration as shown in Figure 2a. The silver nanohole array is covered by the gain medium (R101-PVA film) with a thickness of  $2 \mu\text{m}$  which we have previously reported to exhibit lasing.<sup>[16]</sup> The fitted simulation of the differential transmittance  $\Delta T/T$  and the experimental measurement are shown in Figure 3c.

When the pump power increases, the experimentally measured emission remains at a noise level at first, and then exhibits a well-defined threshold behavior around 2 mW, as shown in Figure 4a. In Figure 4b we simulate the interaction between the electromagnetic fields and the gain medium using the semi-classical framework as explained in detail before. Normalized simulated emission spectra in Figure 4b show a nonlinear increase of the self-emerging emission signal at 617 nm with pump power, in perfect match with the experiment. Thus, the simulations accurately reproduce both the spectral

and threshold behavior of the lasing emission. Furthermore, the calculations uncover the details of the temporal interaction between population inversion and electromagnetic fields in the lasing action. We perform a Fourier transform of the simulated time-domain emission field to obtain the time-averaged field amplitude distribution  $|E(\mathbf{r})|$  at 617 nm and the population inversion  $N_2(\mathbf{r}, t) - N_1(\mathbf{r}, t)$  at different levels of pumping power. For 3.5 mW pumping power (above threshold), the stimulated emission is several orders of magnitude higher than the spontaneously emitted electric fields for 0.5 mW pumping power (below threshold), as shown in Figure 5. These findings confirm that the silver nanohole array supports SPP-Bloch waves which exhibit coherent constructive interference of SPP waves, and they are amplified by the gain medium. We further find that Fabry–Perot modes formed in the gain medium above the silver nanohole array are amplified by 6 orders of magnitude (see Figure 5a,b). The hybridization of SPP-Bloch modes and photonic Fabry–Perot modes minimizes losses in the effective mode volume and supports coherent lasing emission. Below threshold, a high population inversion is achieved in the system in the regions with high electric fields (compare Figures 5a and 6a). On the other hand, when the system is above threshold, the spatial profile of the population density ( $N_2(\mathbf{r}, t) - N_1(\mathbf{r}, t)$ ) inversely correlates with the electromagnetic mode profile because of the inversion depletion by strong lasing fields (compare Figures 5b and 6b). We further plot the temporal dynamics of the population density in the hot spots of electric fields in Figure 6c,d. Below the

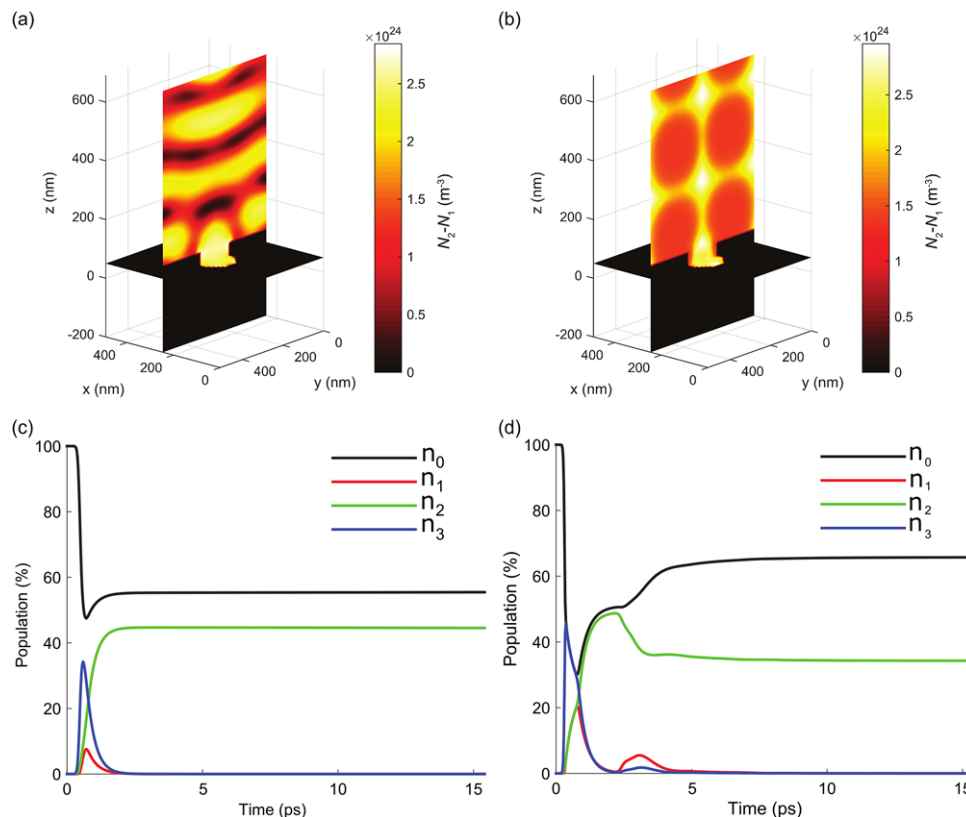


**Figure 6.** The simulated results of the steady-state population inversion distribution ( $N_2 - N_1$ ) for pumping power of a) 0.5 mW and b) 3.5 mW; The time-domain population evolution at the position ( $x = 250 \text{ nm}$ ,  $y = 250 \text{ nm}$ ,  $z = 50 \text{ nm}$ ) for pumping power of c) 0.5 mW and d) 3.5 mW.

lasing threshold, the population of the upper lasing level  $|2\rangle$  stays at 45% (the lower level  $|1\rangle$  is almost empty). However, above the threshold, stimulated transitions in the strong localized electromagnetic fields produced by lasing deplete the population of the excited-state molecules from 48% to 35% of the total population.

### 3.3. Compensation of Losses in Kretschmann–Raether Configuration

In the second study, compensation of the SPP losses in the Kretschmann–Raether configuration<sup>[5]</sup> is analyzed. The retrieved kinetic parameters for the fluorescent green-PMMA film are fitted to the six-level atomic model (Figure 1b) as follows. Transition wavelengths are  $\lambda_{50} = 438$  nm,  $\lambda_{40} = 466$  nm,  $\lambda_{31} = 486$  nm, and  $\lambda_{32} = 513$  nm. Dephasing time for all radiative transition is  $T_2 = 10$  fs and decay times are  $\tau_{r,50} = 13$  ns,  $\tau_{r,40} = 55$  ns,  $\tau_{r,32} = 23$  ns,  $\tau_{r,31} = 84$  ns,  $\tau_{nr,53} = 1$  ps,  $\tau_{nr,43} = 1$  ps,  $\tau_{nr,32} = 300$  ns,  $\tau_{nr,31} = 300$  ns,  $\tau_{nr,30} = 2.9$  ns,  $\tau_{nr,20} = 1$  ps and,  $\tau_{nr,10} = 1$  ps.

The fitted system parameters are fed to a 2D finite difference time-domain (FDTD) analysis of the experimental setup shown in Figure 7a. The structure is composed of a 500-nm layer of the fluorescent green dye in PMMA, coated on top of a 50-nm silver film. The prism is from glass with refractive index of 1.784 and the refractive index of the PMMA host is 1.5. The material properties of silver are taken from Johnson and Christy.<sup>[45]</sup> The dye

is pumped at 438 nm from the backside of the prism while the probe is incident through a glass prism. Pulse width for the pump signal is 1 ps and for the probe signal is 10 fs and the probe signal is delayed by 3 ps. For a 50-nm silver film, the SPP resonance condition at 513 nm corresponds to an incidence angle of  $70.9^\circ$ , which is represented by the dip in the reflectivity curve shown in Figure 7b. The amount of loss compensation (SPP amplification) is function of many factors that control how much gain is introduced to the system.

We study the effects of the concentration  $N$  of dye molecules and the pump energy on the system behavior. The passive system without gain exhibits a dip in reflectivity at 513 nm and incidence angle of  $70.9^\circ$  with minimum reflection  $R_{\min} = 0.063\%$ . Fixing the dye concentration at 1 mM and varying the pump energy, the minimum reflection is enhanced by 11-fold at pump energy of  $0.3 \mu\text{J}$  and can go up to 44.4%, which is about 700-fold enhancement of the SPP dip at pump energy of  $0.5 \text{ mJ}$ , Figure 7b. The relation between  $R_{\min}$  and the pump energy is shown in Figure 7c, which shows almost linear dependence of  $R_{\min}$  on the pump energy. Moreover, the dependence of  $R_{\min}$  on the concentration of dye molecules is plotted in Figure 7d. We can conclude that the enhancement of the reflectivity with the change in concentration of the active media is not as strong as its dependence on the pump energy.  $R_{\min} = 3.83\%$  is observed at dye concentration as high as 100 mM which corresponds approximately to 60-fold enhancement.

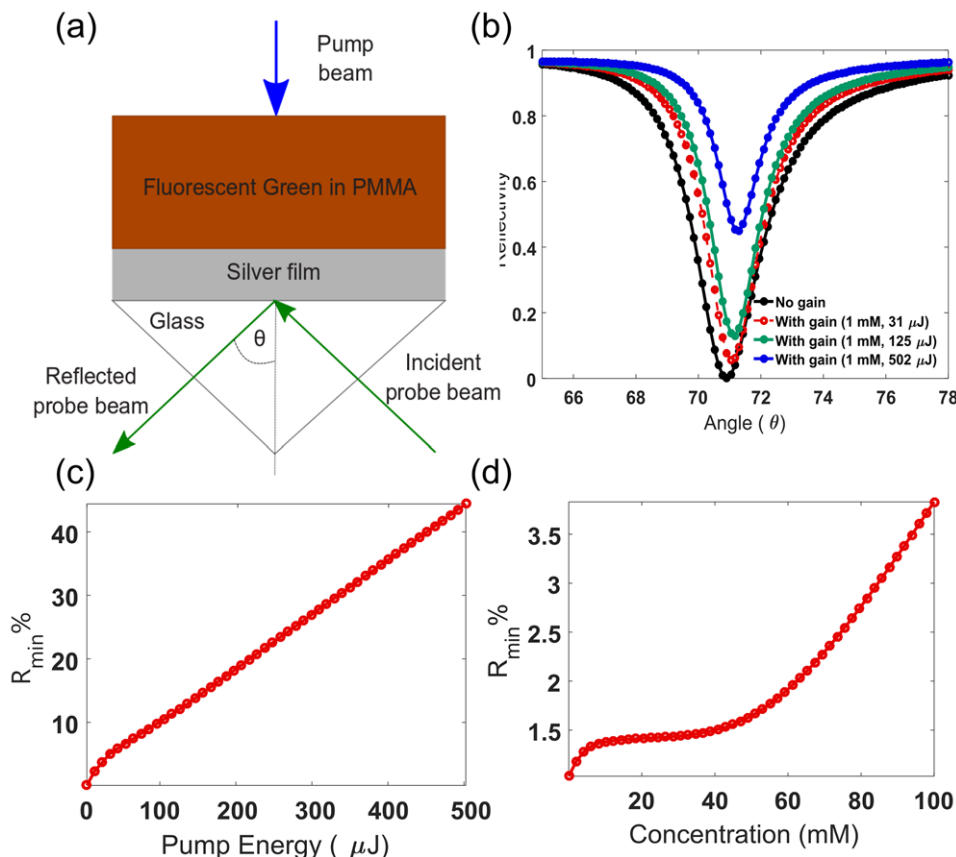


**Figure 7.** a) Schematic of the Kretschmann–Raether SPP excitation configuration. b) Reflectivity at no gain and with gain at different pump energies. Dependence of the reflection minimum ( $R_{\min}$ ) on the c) pump energy, and d) dye molecule concentration.

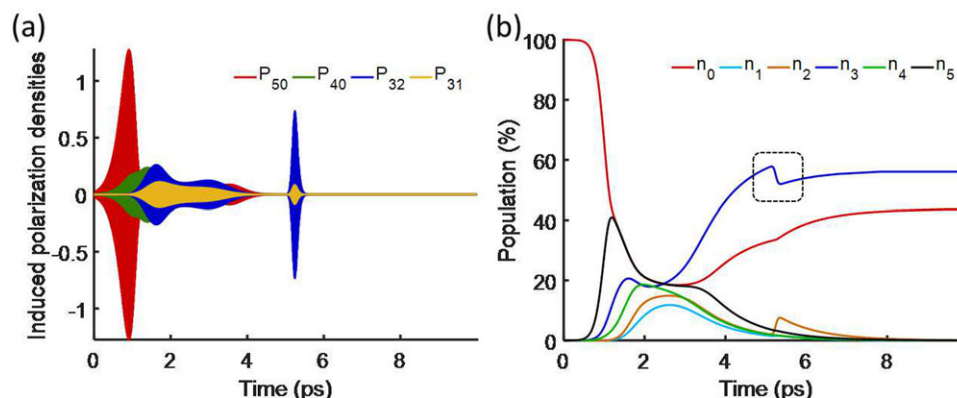


**Figure 8.** Temporal dynamics of the a) induced macroscopic polarizations, and b) population densities at different levels. The dotted rectangle shows the energy transfer between the active medium and the SPP mode which is the essence of the loss compensation/amplification process.

Temporal evolution of the macroscopic polarizations and the population densities at all the six levels are recorded near the silver film and plotted in **Figure 8**. The population inversion is achieved when  $(N_3 - N_2) > 0$ . The highlighted area in Figure 8b shows the depletion of carriers in the upper lasing state  $N_3$  from 57.8% to 52% which correspond to the energy transfer between the stored energy in the dye due to pumping and the SPP, which causes the amplification.

These findings can be elucidated by the frequency domain analysis which shows that the introduction of gain increases the optimal Ag thickness for the minimal zero reflectivity from 50 nm to a thicker film. This minimum “can be thought of as being due to destructive interference between the totally reflected light and the light emitted by the SPP wave due to radiation damping.”<sup>[46]</sup> Gain decreases the internal damping of the surface plasmon on the PMMA-Ag interface. This necessitates the decrease of the “optimal radiative damping” that could be realized by thickening of the Ag layer.<sup>[47]</sup> In addition, gain appreciably narrows the resonance, as the overall absorption of the system and its effective quality factor increase. These effects are observed with small to moderate gain values, insufficient to support reflective “lasing” in such a system.

Plasmon resonance corresponds to 0 in reflectance ( $R$ ), or when the numerator of  $R \rightarrow 0$ . On the other hand, lasing corresponds to the pole in  $R$ , that is, when  $1/R \rightarrow 0$ . Ideally, at higher active medium concentrations the linear reflectivity goes to infinity, while absorption becomes infinitely negative, in full accord with the theory of scattering and absorption of spasers. A correct frequency domain analysis around the threshold should include saturation<sup>[28,29]</sup> that makes all the quantities finite. In the present multiphysics time-domain framework it is taken care of automatically with multi-level kinetic Equation (1) or (4). That makes the proposed numerical framework perfectly suitable for modeling spasers.

## 4. Conclusions

To conclude, we have studied the interaction between the light, plasmons, and gain media using a time-domain multiphysics numerical framework arranged of coupled kinetic equations for

multi-level gain systems. We use calibrated kinetic parameters to investigate net amplification and lasing behavior of two plasmon-enhanced gain systems. Our models predict amplification and fast gain saturation which is induced by strong plasmonic coupling. As the pumping power increases, lasing emission and threshold behavior are obtained for the nanohole array system, which is in excellent agreement with the experiment. The simulation further reveals the temporal details of energy transfer process in the lasing regime. Such detailed and accurate models are necessary for understanding, predicting, and designing new types of nanoscale lasers and gain-compensated plasmonic systems. Based on this systematic approach, further studies could be applied to time-resolved physics of active plasmonic nanostructures. Our numerical framework can serve as a paradigm for in-depth investigation and optimal design of other metadevices coupled with gain. Since the MBL approach has not been implemented in our numerical models as of yet we are planning to include the quantum fluctuations in future efforts specifically dealing with in-depth analysis of numerical metrics pertinent to enhanced spontaneous emission modeling. Future efforts may also include analysis of lasing dynamics in emerging 2D materials.<sup>[48]</sup>

## Acknowledgements

S.I.A., J.F., J.L., and Z.W. equally contributed to this work. The authors acknowledge financial support by DARPA/DSO Extreme Optics and Imaging (EXTREME) Program, Award HR00111720032, Office of Naval Research Grant (MURI N00014-13-0649), ERC Starting Grant 257158 “Active NP”. X.M. is grateful to the financial support by the Incubation Program of Universities’ Preponderant Discipline of Shandong Province, China (No. 03010304) and Mountain Tai Young Scholarship (No. 23170504). N.A. thanks the Linz Institute of Technology (LIT), project ADAPT, and the Austrian Science Fund (FWF), project P 29603, for financial support.

## Conflict of Interest

The authors declare no conflict of interest.

## Keywords

active plasmonics, gain media, lasers, loss compensation, spasers

Received: March 9, 2018

Revised: September 19, 2018

Published online: October 16, 2018

- [1] S. A. Maier, *Plasmonics: Fundamentals and Applications*, Springer, Springer Science & Business Media, Berlin, Germany **2007**.
- [2] M. L. Brongersma, V. M. Shalaev, *Science* **2010**, *328*, 440.
- [3] M. I. Stockman, *J. Opt.* **2010**, *12*, 024004.
- [4] M. Premaratne, M. I. Stockman, *Adv. Opt. Photon.* **2017**, *9*, 79.
- [5] M. A. Noginov, V. A. Podolskiy, G. Zhu, M. Mayy, M. Bahoura, J. A. Adegoke, B. A. Ritzo, K. Reynolds, *Opt. Express* **2008**, *16*, 1385.
- [6] S. Wuestner, A. Pusch, K. L. Tsakmakidis, J. M. Hamm, O. Hess, *Phys. Rev. Lett.* **2010**, *105*, 127401.
- [7] D. J. Bergman, M. I. Stockman, *Phys. Rev. Lett.* **2003**, *90*, 027402.
- [8] F. van Beijnum, P. J. van Veldhoven, E. J. Geluk, M. J. de Dood, W. Gert, M. P. van Exter, *Phys. Rev. Lett.* **2013**, *110*, 206802.
- [9] M. A. Noginov, G. Zhu, A. M. Belgrave, R. Bakker, V. M. Shalaev, E. E. Narimanov, S. Stout, E. Herz, T. Suteewong, U. Wiesner, *Nature* **2009**, *460*, 1110.
- [10] Z. Wang, X. Meng, A. V. Kildishev, A. Boltasseva, V. M. Shalaev, *Laser Photonics Rev.* **2017**, *11*, 1700212.
- [11] R. F. Oulton, V. J. Sorger, T. Zentgraf, R. M. Ma, C. Gladden, L. Dai, G. Bartal, X. Zhang, *Nature* **2009**, *461*, 629.
- [12] T. P. Sidiropoulos, R. Röder, S. Geburt, O. Hess, S. A. Maier, C. Rönning, R. F. Oulton, *Nat. Phys.* **2014**, *10*, 870.
- [13] M. Khajavikhan, A. Simic, M. Katz, J. H. Lee, B. Slutsky, A. Mizrahi, V. Lomakin, Y. Fainman, *Nature* **2012**, *482*, 204.
- [14] W. Zhou, M. Dridi, J. Y. Suh, C. H. Kim, D. T. Co, M. R. Wasielewski, G. C. Schatz, T. W. Odom, *Nat. Nanotech.* **2013**, *8*, 506.
- [15] F. van Beijnum, P. J. van Veldhoven, E. J. Geluk, M. J. de Dood, W. Gert, M. P. van Exter, *Phys. Rev. Lett.* **2013**, *110*, 206802.
- [16] X. Meng, J. Liu, A. V. Kildishev, V. M. Shalaev, *Laser Photonics Rev.* **2014**, *8*, 896.
- [17] T. Pickering, J. M. Hamm, A. F. Page, S. Wuestner, O. Hess, *Nat. Commun.* **2014**, *5*, 4972.
- [18] S. Wuestner, J. M. Hamm, A. Pusch, O. Hess, *Laser Photonics Rev.* **2015**, *9*, 256.
- [19] A. Scherer, J. Vučković, M. Loncar, U.S. Patent 6,534,798, **2003**.
- [20] J. Vučković, M. Loncar, A. Scherer, *IEEE J. Quantum Electron.* **2000**, *36*, 1131.
- [21] H. R. Stuart, U.S. Patent 6,836,494, **2004**.
- [22] J. Stehr, J. Crewett, F. Schindler, R. Sperling, G. Von Plessen, U. Lemmer, J. M. Lupton, T. A. Klar, J. Feldmann, A. W. Holleitner, M. Forster, *Adv. Mater.* **2003**, *15*, 1726.
- [23] S. I. Azzam, N. Arnold, L. Prokopenko, Z. Kudyshev, A. V. Kildishev, in *Frontiers in Optics 2016*, Optical Society of America, Rochester, NY, USA **2016**, JW4A.132.
- [24] I. De Leon, P. Berini, *Nat. Photonics* **2010**, *4*, 382.
- [25] N. Meinzer, M. Ruther, S. Linden, C. M. Soukoulis, G. Khitrova, J. Hendrickson, J. D. Orlitzky, H. M. Gibbs, M. Wegener, *Opt. Express* **2010**, *18*, 24140.
- [26] Z. Huang, T. Koschny, C. M. Soukoulis, *Phys. Rev. Lett.* **2012**, *108*, 187402.
- [27] S. Xiao, V. P. Drachev, A. V. Kildishev, X. Ni, U. K. Chettiar, H.-K. Yuan, V. M. Shalaev, *Nature* **2010**, *466*, 735.
- [28] N. Arnold, C. Hrelescu, T. A. Klar, *Ann. Phys.* **2016**, *528*, 295.
- [29] N. Arnold, K. Pigmayer, A. V. Kildishev, T. A. Klar, *Opt. Mater. Express* **2015**, *5*, 2546.
- [30] G. V. Kristanz, N. Arnold, A. V. Kildishev, T. A. Klar, *ACS Photonics* **2018**, *5*, 3695.
- [31] M. I. Stockman, *Phys. Rev. Lett.* **2011**, *106*, 156802.
- [32] M. Dridi, G. C. Schatz, *J. Opt. Soc. Am.* **2013**, *30*, 2791.
- [33] E. I. Smotrova, A. I. Nosich, T. M. Benson, P. Sewell, *IEEE J. Sel. Top. Quantum Electron.* **2005**, *11*, 1135.
- [34] A. Taflove, S. Hagness, *Computational Electrodynamics: The Finite-Difference Time-Domain Method*, Artech House, Norwood, MA **2005**.
- [35] T. Matsui, M. Kitaguchi, *Appl. Phys. Express* **2010**, *3*, 061701.
- [36] A. Fang, T. Koschny, C. M. Soukoulis, *J. Opt.* **2010**, *12*, 024013.
- [37] H. Alaeian, B. C. Odom, J. Bravo-Abad, *Ann. Phys.* **2018**, *1800203*, <https://doi.org/10.1002/andp.201800203>.
- [38] A. Pusch, S. Wuestner, J. M. Hamm, K. L. Tsakmakidis, O. Hess, *ACS Nano* **2012**, *6*, 2420.
- [39] S. Wuestner, J. M. Hamm, A. Pusch, F. Renn, K. L. Tsakmakidis, O. Hess, *Phys. Rev. B* **2012**, *85*, 201406.
- [40] S. Wuestner, T. Pickering, J. M. Hamm, A. F. Page, A. Puscha, O. Hess, *Faraday Discuss.* **2015**, *178*, 307.
- [41] J. Trieschmann, S. Xiao, L. J. Prokopenko, V. P. Drachev, A. V. Kildishev, *Opt. Express* **2011**, *19*, 18253.
- [42] B. Ding, C. Hrelescu, N. Arnold, G. Isic, T. A. Klar, *Nano Lett.* **2013**, *13*, 378.
- [43] L. J. Prokopenko, J. D. Borneman, A. V. Kildishev, *IEEE Trans. Mag.* **2011**, *47*, 1150.
- [44] X. Ni, Z. Liu, A. V. Kildishev, *PhotonicsDB: Optical Constants* **2008**, <https://doi.org/10.4231/D3FT8DJ4>.
- [45] P. B. Johnson, R. W. Christy, *Phys. Rev. B* **1972**, *6*, 4370.
- [46] L. Novotny, B. Hecht, *Principles of Nano-Optics*, Cambridge University Press, Cambridge, UK **2012**, p. 387.
- [47] H. Raether, *Surface Plasmons on Smooth and Rough Surfaces and on Gratings*, Springer-Verlag, Berlin, New York **1988**, p. 12, Eqns. (2.24), (2.22), and (2.19).
- [48] H. Fang, J. Liu, H. Li, L. Zhou, L. Liu, J. Li, X. Wang, T. F. Krauss, Y. Wang, *Laser Photonics Rev.* **2018**, *12*, 1800015.